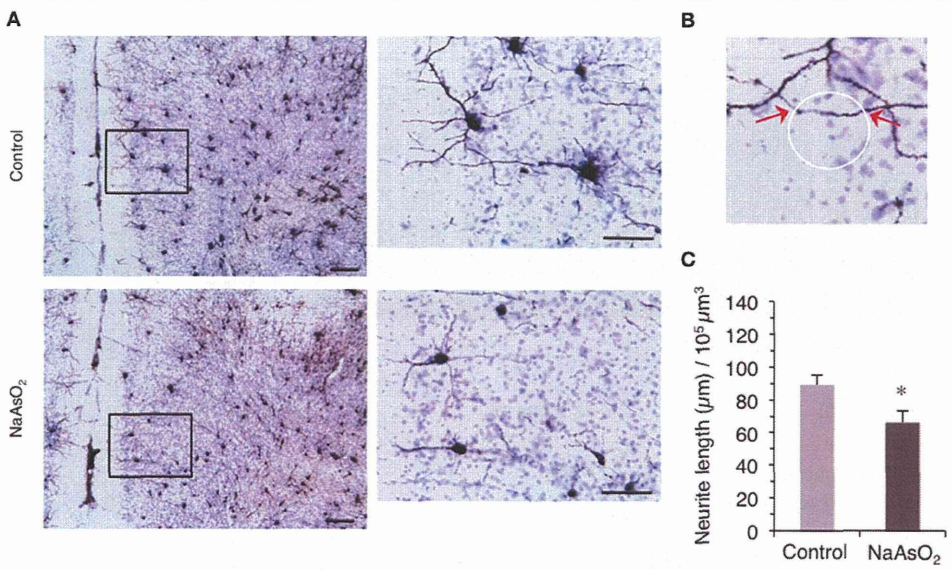

FIGURE 3 | Altered morphology of neurites in the PrL of adult female mice born to dams that were administered $NaAsO_2$ during gestation. (A) Representative photomicrographs of the PrL in Golgi- and Cresyl Fast Violet-stained coronal brain sections from female mice with or without prenatal exposure to $NaAsO_2$. The rectangular area was magnified and shown in the corresponding right panel. Bars = 20 μm (low magnification) and 10 μm (high magnification). **(B)** Demonstrative photomicrograph for the intersection points (indicated by red arrows) between a virtual sphere "Space Ball" (white circle) and Gogli-stained neurite. **(C)** Estimated neurite lengths in Golgi-stained PrL neurons as measured by the Space Ball method. Values (mean ± SEM) were normalized to the estimated volume of the selected PrL region (control group $n = 7$, $NaAsO_2$-exposed group $n = 5$). An asterisk indicates $p < 0.05$ vs. the control group.

control and $NaAsO_2$-exposed groups in any observed layer of the PrL (**Figures 4C–E**).

DISCUSSION

In the present study, we investigated the effect of prenatal $NaAsO_2$ exposure on the behavioral flexibility/reversal learning of adult mice using the IntelliCage system, which is an efficient tool for monitoring multiple aspects of cognitive behavior in a social environment (Endo et al., 2012; Benner et al., 2015). The core finding of our work is that exposure of dams to $NaAsO_2$ produces behavioral inflexibility to reversal learning and abnormal formation of the PrL in adult offspring. These findings suggest that behavioral impairments caused by $NaAsO_2$ exposure are associated with structural changes of brain, particularly in the PrL cortical region.

Here, we provided pregnant female mice with drinking water that contained 85 ppm $NaAsO_2$ during a critical period of embryonic brain development (gestational day 8–18). A series of studies by Colomina et al. evaluated the effect of $NaAsO_2$ exposure on development of nervous system. Exposure to $NaAsO_2$ at 10 mg/kg/day throughout gestational day 15–18 delayed neurodevelopmental indices such as eye opening in female offspring (Colomina et al., 1997). Furthermore, they have shown that single $NaAsO_2$ exposure at 30 mg/kg induces deficit in neuromotor development (Colomina et al., 1996). In accordance with these studies, we considered that providing $NaAsO_2$ about 10 mg/kg to pregnant mice during gestation might induce higher brain function deficits in offspring. It has been reported that mice drink around 5 ml of water daily (Bachmanov et al., 2002). However, our own measurement showed that a 25–35 g pregnant mouse drink about 3.5 ml of water daily when the mouse is provided with $NaAsO_2$-containing water (Figure S5). Based on these estimates, a 25–35 g dam consumes 0.39 mg $NaAsO_2$/day (which is equivalent to 8.5–12 mg/kg/day) when dams are provided with drinking water containing 85 ppm $NaAsO_2$. The selected $NaAsO_2$ dose used in the current study did not produce any obvious maternal toxicity or embryonic toxicity (Figures S1, S2), which is consistent with the previous studies (Rodriguez et al., 2002; Waalkes et al., 2003; Markowski et al., 2012).

Behavioral flexibility describes the ability of an organism to adapt to a changing environment. Behavioral flexibility occurs in many kinds of animal, such as mice, rat, and monkey, and is often assessed using rule-shift learning task paradigms that include a sequencing reversal task. In this study, we assessed the behavioral flexibility of control or $NaAsO_2$-exposed female mice using an altered action-outcome contingency paradigm during inter-sessions, and inter-reversal stages that included a serial reversal task (Endo et al., 2012). In the inter-session analysis, day-to-day improvements in adaptive behavior, as observed in a decreasing trend of discrimination error rate in each reversal phase, were clearly observed not only in control but also arsenite-exposed groups. However, $NaAsO_2$-exposed mice demonstrated a lower degree of achievement in reversal learning than the control group. It may be inferred that the repetition of reversal learning lead to difficultly in re-acquiring reversal learning for the $NaAsO_2$-exposed group. Such effects of arsenic have

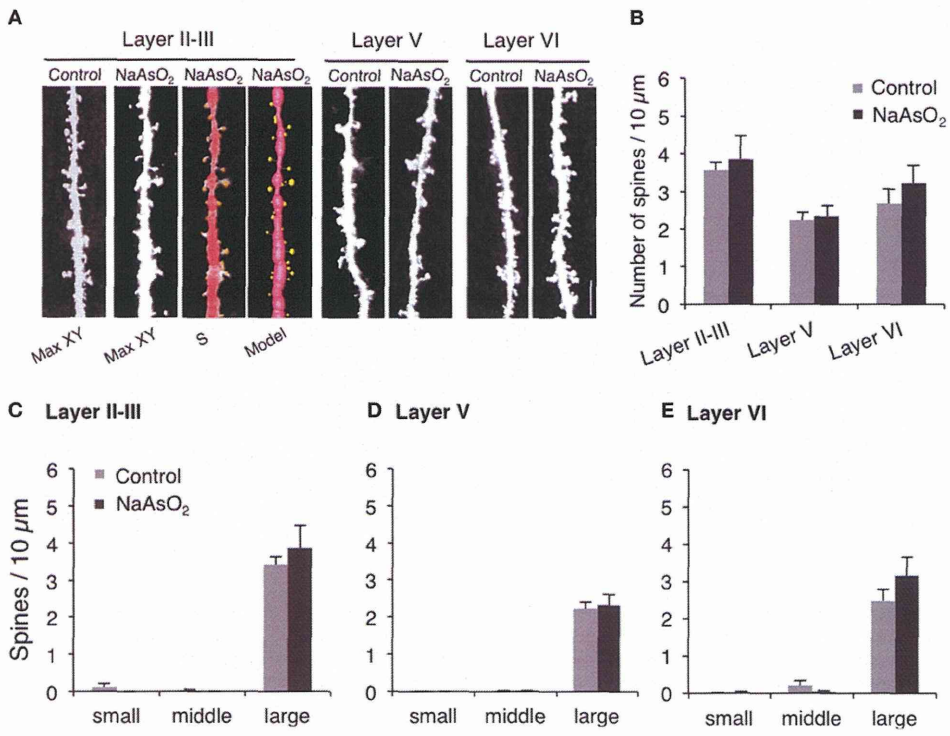

FIGURE 4 | The density and the morphology of dendritic spines in the PrL of adult female mice born from dams exposed to $NaAsO_2$ during gestation. Dendritic spines were analyzed along the primary basilar dendrites of Golgi-stained pyramidal neurons in three different cortical layers (layer II–III, V, and VI) of PrL. **(A)** Representative photomicrographs of dendritic spines with maximal intensity projections onto the XY plane from Z-series images (Max-XY) for the control group (Control) and $NaAsO_2$-exposed group. Photomicrographs analyzed by Spiso-3D (S) and three-dimensional models (Model) are also shown for the analysis of dendritic spines in the layer II–III of the $NaAsO_2$-exposed group. **(B)** Effect of $NaAsO_2$ exposure on the total dendritic spine density of pyramidal neurons in three different cortical layers. Effect of $NaAsO_2$ exposure on the density of three subtypes of dendritic spines, small-head spines (small), middle-head spines (middle), and large-head spines (large), in three cortical layers of the PrL: Layer II–III **(C)**, Layer V **(D)**, and Layer VI **(E)**. The density of dendritic spines is expressed as the number of spines per 10 μm of dendrite. A total 500–1200 spines from 30 to 45 dendritic segments of 30–45 neurons were analyzed for each cortical layer. Values are expressed as mean ± SEM (control group $n = 7$, $NaAsO_2$-exposed group $n = 5$).

been reported in adulthood exposure. A series of studies have demonstrated that arsenic exposure in adult mice produces an increase in the number of errors in an egocentric task (Rodriguez et al., 2001, 2002). Our present findings suggest that $NaAsO_2$ exposure in early life also produces behavioral impairments in learning function in mice. The first session of each reversal stage in the serial reversal-learning task tests the ability of mice to adapt to a changing task, because in this first session, mice must alter their behavioral sequence in order to receive a reward. Mice in the control group adapted to new behavioral sequences after a series of reversals, whereas mice in the $NaAsO_2$-exposed group did not adequately adapt to changing tasks (**Figure 1E**) that was likely indicative of behavioral inflexibility.

We also revealed a possible link between behavioral alterations and structural changes in the PrL cortical region. The PrL is known to be involved in the regulation of cognitive and executive processes (Dalley et al., 2004; Marquis et al., 2007; Ragozzino, 2007). It has been demonstrated that the PrL plays a fundamental role in behavioral flexibility. For example, patients who have the frontal lobe (including PrL) damage show impaired adaptation to changes in reinforcement contingencies in spite of the fact that these patients can acquire novel skills or adopt new rules with relative ease (Owen et al., 1993). It has also demonstrated that either lesion or inactivation of the PrL impairs behavioral flexibility in rodents (Ragozzino et al., 1999). Accordingly, structural changes in the PrL can contribute to the impairment of behavioral flexibility. $NaAsO_2$ is known to produce neurotoxicity by inducing apoptotic cell death (Wong et al., 2005; Keim et al., 2012) and/or cellular necrosis (Chattopadhyay et al., 2002; Yang et al., 2003). Therefore, in the present study, we measured the number of neurons and glial cells in the PrL in order to determine whether cell viability was affected by prenatal $NaAsO_2$ exposure. Contrary to our expectations, these morphometrical analyses revealed that $NaAsO_2$ exposure increased the number of pyramidal neurons in layers V and VI of the PrL (**Figure 2D**). Our previous *in vitro* work showed that a high concentration of $NaAsO_2$ (2 μM) reduced the viability of mouse primary cortical neurons, but that a low concentration of $NaAsO_2$ (0.5 μM) conversely increased cell viability and promoted cellular proliferation (Maekawa et al., 2013). It suggests

that the concentration of $NaAsO_2$ (85 ppm) used in the present study reflect the low concentration of $NaAsO_2$ exposure resulting in the increase in the number of pyramidal neurons in the present. On the other hand, the number of non-pyramidal neurons and glial cells was not affected by $NaAsO_2$ exposure in the present study. The difference between the effect of $NaAsO_2$ exposure on pyramidal and non-pyramidal cells (**Figures 2D,E**) could be due to differences in the timing of neurogenesis and neuronal migration. The majority of cerebral cortical neurons are generated during embryonic day 11–17 in mouse (Price and Lotto, 1996; Price et al., 1997), whereas neurogenesis for each cortical layer is not simultaneous and occurs with variable timing (Finlay and Darlington, 1995). Additionally, pyramidal neurons are generated from the ventricular zone and migrate through the cortical layers radially, while interneurons including non-pyramidal neurons are generated from the ganglionic eminence and migrate tangentially (Nadarajah et al., 2003). Therefore, the timing of generation and migration of pyramidal neurons is different from that of non-pyramidal neurons, and these differences may reflect the layer-specific and cell type-specific effects of $NaAsO_2$ on the number of neurons in the PrL observed in the present study. Several studies have already shown that chemical exposures affect neuronal migration by disrupting the inside-out pattern of migration (Kakita et al., 2002; Schreiber et al., 2010). Taken together, the generation and migration of neurons may be at least partially affected by prenatal $NaAsO_2$ exposure, although the mechanisms by which $NaAsO_2$ exposure specifically increases the number of pyramidal neurons in a layer-dependent manner has not yet been identified. Regarding glial cells, morphological or functional changes have been shown to occur at higher $NaAsO_2$ concentrations than those, which affect the morphology of neurons (Wang et al., 2012). Therefore, the observed lack of effect of $NaAsO_2$ exposure on the number of glial cells in this study was expected, and may be due to an insufficient level of prenatal $NaAsO_2$ exposure.

Another critical finding of our study is that behavioral inflexibility is clearly associated with structural changes in PrL neurons. We previously demonstrated that $NaAsO_2$ disrupts neuritogenesis in primary cultured neurons (Maekawa et al., 2013) and neuronal cell lines (Aung et al., 2013), and that inhibition of neuritogenesis by $NaAsO_2$ is caused by alterations in the expression of cytoskeletal genes, tau, tubulin, and neurofilament (Aung et al., 2013), and suppression of glutamate AMPA receptor expression (Maekawa et al., 2013). Thus, inorganic arsenic adversely affects the fate and maturation processes of young neurons, which may lead to abnormal formation of neural circuits. In the present study, we found that the length of neurites in the PrL was significantly lower in the $NaAsO_2$-exposed group, suggesting that prenatal exposure to $NaAsO_2$ has an adverse effect on neuritogenesis. Elongation of the axon and dendrites is an essential event for the formation of basic neuronal circuitry. Impairments in the length and morphology of dendrites in the frontal cortex are involved in the pathogenesis of cognitive deficits and mental retardation (Armstrong et al., 1998). It indicates that the alteration in the morphology of neuron, particularly the PrL neuron, is strongly associated with the pathophysiological states of cognitive and learning dysfunction and that prenatal exposure to $NaAsO_2$ may contribute to the pathogenesis. Additionally, it has been reported that the degree of learning disability is positively correlated with the severity and extent of dendritic abnormalities (Kaufmann and Moser, 2000). Therefore, we subsequently examined the density and morphology of pyramidal neuron dendritic spines in different layers of the PrL. In contrast to the impairment in neurite length, the morphology and the density of dendritic spines in PrL pyramidal neurons were not affected by $NaAsO_2$ exposure. We recently demonstrated in cultured neurons that $NaAsO_2$ specifically alters the gene expression of cytoskeletal proteins including tau, tubulin, and neurofilaments, but does not affect the expression of actin protein (Aung et al., 2013). Since dendritic spines are actin-rich protrusions from dendrites that form the post-synaptic component of a synapse (Hotulainen and Hoogenraad, 2010), our current finding that $NaAsO_2$ exposure did not have an effect on synapse number agrees with our previous study regarding the expression of actin protein. $NaAsO_2$ exposure has however been reported to impair the expression of AMPA and NMDA glutamate receptors (Maekawa et al., 2013; Ramos-Chavez et al., 2015), suggesting that $NaAsO_2$ exposure can affect glutamate transmission. Because glutamate transmission is critically involved in the regulation of synapse formation (Rasse et al., 2005), we cannot exclude the possibility that the exposure to $NaAsO_2$ alters synapse formation in areas other than the PrL. Taken together, the present study highlights the possible association between behavioral impairment in mice caused by prenatal $NaAsO_2$ exposure and morphological alteration of brain, particularly cortical disarrangement in the prelimbic cortex.

On the other hand, the suggested association between the behavioral inflexibility and morphological alteration of the PrL was come from the morphometrical analysis, which was however carried out following the behavioral flexibility test. It has been demonstrated in human subjects that goal-directed learning is strongly associated with increase neural activity in prefrontal cortex (Valentin et al., 2007) and higher neurite density in medial orbitofrontal cortex (Morris et al., 2016). Since the control mice performed better than $NaAsO_2$-exposed mice in this study of behavioral flexibility tasks, we could not deny the possibility of increase neurite length in the PrL of the control mice, which might be outcome of better goal-directed learning in behavioral flexibility tasks. In addition, it is important to note that the reduced maternal water consumption was observed in the group of dams provided with water containing $NaAsO_2$, and the difference between the two groups was about 2 ml per day (Figure S5). It might be due to unpalatability of dams to water containing $NaAsO_2$. Although we did not observe the obvious signs of maternal or embryonic toxicity such as maternal weight (Figure S1) and the number of pups (Figure S2) between the two groups of this study, several studies reported the possibility that maternal dehydration due to reduced water intake during pregnancy was associated with long-term physiologic effects on offspring such as development of brain function and plasma composition (Desai et al., 2005; Ross et al., 2005; Zhang et al., 2011). Therefore, we had to assume that behavioral inflexibility observed in mice prenatally

exposed $NaAsO_2$ could be induced by the combinatorial effect of the toxicity of prenatal $NaAsO_2$ exposure and maternal dehydration.

In this study, we used male and female mice at 67 week (15.5 month) of their age in this study of behavioral flexibility tests, which additionally lasted for 10–12 weeks (about 2–3 month). Therefore, the age of mice in the last day of behavioral tests was being 17.5–18.5 month, which could be generally considered as old aged mice. It has been demonstrated that arsenic-induced increase in oxidative stress (such as glutathione level in the blood) was more prominent in young and old rats compared to adults (Jain et al., 2011, 2012). Motor impairments caused by prenatal arsenic exposure were observed in young juvenile mice, but such effects observed in young mice were subsided with advancing age (Markowski et al., 2012). These studies indicate age-dependent effects of arsenic-induced toxicity. Therefore, although we observed $NaAsO_2$-induced behavioral inflexibility in old aged mice in the present study, we need further studies to test the age-dependent effects of prenatal $NaAsO_2$ exposure on behavioral flexibility.

In conclusion, we demonstrate the possibility that *in utero* $NaAsO_2$ exposure leads to behavioral inflexibility to changing tasks in adulthood, and cortical disarrangement in the PrL might contribute to this behavioral impairment. Further studies are required to elucidate how $NaAsO_2$ disrupts neuronal development including axonal and dendritic elongation particularly in prefrontal cortex. Since behavioral inflexibility is observed in children with neurodevelopmental disorders such as autism spectrum disorders, our findings put forth a new perspective on how environmental exposures affect the pathogenesis of neurodevelopmental disorders.

AUTHOR CONTRIBUTIONS

KA designed and performed experiments, analyzed data and wrote the paper; CT, KS performed experiments and analyzed data; KaN, AT, KeN, MK, and CT edited the paper; ST designed experiments and edited the paper; and FM designed experiments, analyzed data and wrote the paper.

ACKNOWLEDGMENTS

This work was supported by JSPS KAKENHI 24590307 to FM, 23310043 to ST, FM, 15K14556 to ST and 24221003 to CT, by the National Institute for Environmental Studies [14309][14013] to FM, and in part by The Grant of National Center for Child Health and Development (25-3) to KN and by the Health Labour Sciences Research Grant from The Ministry of Health Labour and Welfare, Japan to MK.

SUPPLEMENTARY MATERIAL

The Supplementary Material for this article can be found online at: http://journal.frontiersin.org/article/10.3389/fnins.2016.00137

REFERENCES

Armstrong, D. D., Dunn, K., and Antalffy, B. (1998). Decreased dendritic branching in frontal, motor and limbic cortex in Rett syndrome compared with trisomy 21. *J. Neuropathol. Exp. Neurol.* 57, 1013–1017. doi: 10.1097/00005072-199811000-00003

Aung, K. H., Kurihara, R., Nakashima, S., Maekawa, F., Nohara, K., Kobayashi, T., et al. (2013). Inhibition of neurite outgrowth and alteration of cytoskeletal gene expression by sodium arsenite. *Neurotoxicology* 34, 226–235. doi: 10.1016/j.neuro.2012.09.008

Bachmanov, A. A., Reed, D. R., Beauchamp, G. K., and Tordoff, M. G. (2002). Food intake, water intake, and drinking spout side preference of 28 mouse strains. *Behav. Genet.* 32, 435–443. doi: 10.1023/A:1020884312053

Benner, S., Endo, T., Kakeyama, M., and Tohyama, C. (2015). Environmental insults in early life and submissiveness later in life in mouse models. *Front. Neurosci.* 9:91. doi: 10.3389/fnins.2015.00091

Bisen-Hersh, E. B., Farina, M., Barbosa, F. Jr., Rocha, J. B., and Aschner, M. (2014). Behavioral effects of developmental methylmercury drinking water exposure in rodents. *J. Trace Elem. Med. Biol.* 28, 117–124. doi: 10.1016/j.jtemb.2013.09.008

Chaineau, E., Binet, S., Pol, D., Chatellier, G., and Meininger, V. (1990). Embryotoxic effects of sodium arsenite and sodium arsenate on mouse embryos in culture. *Teratology* 41, 105–112. doi: 10.1002/tera.1420410111

Chattopadhyay, S., Bhaumik, S., Purkayastha, M., Basu, S., Nag Chaudhuri, A., and Das Gupta, S. (2002). Apoptosis and necrosis in developing brain cells due to arsenic toxicity and protection with antioxidants. *Toxicol. Lett.* 136, 65–76. doi: 10.1016/S0378-4274(02)00282-5

Colomina, M. T., Albina, M. L., and Domingo, J. L. (1996). Influence of maternal restraint stress on arsenic-induced pre- and postnatal alterations in mice. *Psychobiology* 24, 227–234.

Colomina, M. T., Albina, M. L., Domingo, J. L., and Corbella, J. (1997). Influence of maternal stress on the effects of prenatal exposure to methylmercury and arsenic on postnatal development and behavior in mice: a preliminary evaluation. *Physiol. Behav.* 61, 455–459. doi: 10.1016/S0031-9384(96)00462-3

Dakeishi, M., Murata, K., and Grandjean, P. (2006). Long-term consequences of arsenic poisoning during infancy due to contaminated milk powder. *Environ. Health* 5, 31. doi: 10.1186/1476-069X-5-31

Dalley, J. W., Cardinal, R. N., and Robbins, T. W. (2004). Prefrontal executive and cognitive functions in rodents: neural and neurochemical substrates. *Neurosci. Biobehav. Rev.* 28, 771–784. doi: 10.1016/j.neubiorev.2004.09.006

Desai, M., Gayle, D., Kallichanda, N., and Ross, M. G. (2005). Gender specificity of programmed plasma hypertonicity and hemoconcentration in adult offspring of water-restricted rat dams. *J. Soc. Gynecol. Investig.* 12, 409–415. doi: 10.1016/j.jsgi.2005.04.007

Endo, T., Kakeyama, M., Uemura, Y., Haijima, A., Okuno, H., Bito, H., et al. (2012). Executive function deficits and social-behavioral abnormality in mice exposed to a low dose of dioxin in utero and via lactation. *PLoS ONE* 7:e50741. doi: 10.1371/journal.pone.0050741

Endo, T., Maekawa, F., Voikar, V., Haijima, A., Uemura, Y., Zhang, Y., et al. (2011). Automated test of behavioral flexibility in mice using a behavioral sequencing task in IntelliCage. *Behav. Brain Res.* 221, 172–181. doi: 10.1016/j.bbr.2011.02.037

Ferraro, L., Tomasini, M. C., Tanganelli, S., Mazza, R., Coluccia, A., Carratu, M. R., et al. (2009). Developmental exposure to methylmercury elicits early cell death in the cerebral cortex and long-term memory deficits in the rat. *Int. J. Dev. Neurosci.* 27, 165–174. doi: 10.1016/j.ijdevneu.2008.11.004

Finlay, B. L., and Darlington, R. B. (1995). Linked regularities in the development and evolution of mammalian brains. *Science* 268, 1578–1584. doi: 10.1126/science.7777856

Franklin, K., and Paxinos, G. (2008). *The Mouse Brain in Stereotaxic Coordinates, Compact, 3rd Edn.* Amsterdam: Elsevier Academic Press.

Grandjean, P., and Landrigan, P. J. (2006). Developmental neurotoxicity of industrial chemicals. *Lancet* 368, 2167–2178. doi: 10.1016/S0140-6736(06)69665-7

Grandjean, P., and Landrigan, P. J. (2014). Neurobehavioural effects of developmental toxicity. *Lancet Neurol.* 13, 330–338. doi: 10.1016/S1474-4422(13)70278-3

Hill, E. L., and Bird, C. M. (2006). Executive processes in Asperger syndrome: patterns of performance in a multiple case series. *Neuropsychologia* 44, 2822–2835. doi: 10.1016/j.neuropsychologia.2006.06.007

Hirner, A. V., and Rettenmeier, A. W. (2010). Methylated metal(loid) species in humans. *Met. Ions Life Sci.* 7, 465–521. doi: 10.1039/9781849730822-00465

Hotulainen, P., and Hoogenraad, C. C. (2010). Actin in dendritic spines: connecting dynamics to function. *J. Cell Biol.* 189, 619–629. doi: 10.1083/jcb.201003008

Jain, A., Flora, G. J., Bhargava, R., and Flora, S. J. (2012). Influence of age on arsenic-induced oxidative stress in rat. *Biol. Trace Elem. Res.* 149, 382–390. doi: 10.1007/s12011-012-9432-7

Jain, A., Yadav, A., Bozhkov, A. I., Padalko, V. I., and Flora, S. J. (2011). Therapeutic efficacy of silymarin and naringenin in reducing arsenic-induced hepatic damage in young rats. *Ecotoxicol. Environ. Saf.* 74, 607–614. doi: 10.1016/j.ecoenv.2010.08.002

Kakita, A., Inenaga, C., Sakamoto, M., and Takahashi, H. (2002). Neuronal migration disturbance and consequent cytoarchitecture in the cerebral cortex following transplacental administration of methylmercury. *Acta Neuropathol.* 104, 409–417. doi: 10.1007/s00401-002-0571-3

Kaufmann, W. E., and Moser, H. W. (2000). Dendritic anomalies in disorders associated with mental retardation. *Cereb. Cortex* 10, 981–991. doi: 10.1093/cercor/10.10.981

Keim, A., Rossler, O. G., Rothhaar, T. L., and Thiel, G. (2012). Arsenite-induced apoptosis of human neuroblastoma cells requires p53 but occurs independently of c-Jun. *Neuroscience* 206, 25–38. doi: 10.1016/j.neuroscience.2012.01.001

Kipp, K. (2005). A developmental perspective on the measurement of cognitive deficits in attention-deficit/hyperactivity disorder. *Biol. Psychiatry* 57, 1256–1260. doi: 10.1016/j.biopsych.2005.03.012

Koike-Kuroda, Y., Kakeyama, M., Fujimaki, H., and Tsukahara, S. (2010). Use of live imaging analysis for evaluation of cytotoxic chemicals that induce apoptotic cell death. *Toxicol. In vitro* 24, 2012–2020. doi: 10.1016/j.tiv.2010.07.022

Li, D., Lu, C., Wang, J., Hu, W., Cao, Z., Sun, D., et al. (2009). Developmental mechanisms of arsenite toxicity in zebrafish (Danio rerio) embryos. *Aquat. Toxicol.* 91, 229–237. doi: 10.1016/j.aquatox.2008.11.007

Maekawa, F., Tsuboi, T., Oya, M., Aung, K. H., Tsukahara, S., Pellerin, L., et al. (2013). Effects of sodium arsenite on neurite outgrowth and glutamate AMPA receptor expression in mouse cortical neurons. *Neurotoxicology* 37, 197–206. doi: 10.1016/j.neuro.2013.05.006

Markowski, V. P., Reeve, E. A., Onos, K., Assadollahzadeh, M., and Mckay, N. (2012). Effects of prenatal exposure to sodium arsenite on motor and food-motivated behaviors from birth to adulthood in C57BL6/J mice. *Neurotoxicol. Teratol.* 34, 221–231. doi: 10.1016/j.ntt.2012.01.001

Marquis, J. P., Killcross, S., and Haddon, J. E. (2007). Inactivation of the prelimbic, but not infralimbic, prefrontal cortex impairs the contextual control of response conflict in rats. *Eur. J. Neurosci.* 25, 559–566. doi: 10.1111/j.1460-9568.2006.05295.x

Martínez-Finley, E. J., Ali, A. M., and Allan, A. M. (2009). Learning deficits in C57BL/6J mice following perinatal arsenic exposure: consequence of lower corticosterone receptor levels? *Pharmacol. Biochem. Behav.* 94, 271–277. doi: 10.1016/j.pbb.2009.09.006

Morris, L. S., Kundu, P., Dowell, N., Mechelmans, D. J., Favre, P., Irvine, M. A., et al. (2016). Fronto-striatal organization: defining functional and microstructural substrates of behavioural flexibility. *Cortex* 74, 118–133. doi: 10.1016/j.cortex.2015.11.004

Mouton, P. R., Gokhale, A. M., Ward, N. L., and West, M. J. (2002). Stereological length estimation using spherical probes. *J. Microsc.* 206, 54–64. doi: 10.1046/j.1365-2818.2002.01006.x

Mukai, H., Hatanaka, Y., Mitsuhashi, K., Hojo, Y., Komatsuzaki, Y., Sato, R., et al. (2011). Automated analysis of spines from confocal laser microscopy images: application to the discrimination of androgen and estrogen effects on spinogenesis. *Cereb. Cortex* 21, 2704–2711. doi: 10.1093/cercor/bhr059

Nadarajah, B., Alifragis, P., Wong, R. O., and Parnavelas, J. G. (2003). Neuronal migration in the developing cerebral cortex: observations based on real-time imaging. *Cereb. Cortex* 13, 607–611. doi: 10.1093/cercor/13.6.607

Owen, A. M., Roberts, A. C., Hodges, J. R., Summers, B. A., Polkey, C. E., and Robbins, T. W. (1993). Contrasting mechanisms of impaired attentional set-shifting in patients with frontal lobe damage or Parkinson's disease. *Brain* 116(Pt 5), 1159–1175. doi: 10.1093/brain/116.5.1159

Price, D. J., Aslam, S., Tasker, L., and Gillies, K. (1997). Fates of the earliest generated cells in the developing murine neocortex. *J. Comp. Neurol.* 377, 414–422.

Price, D. J., and Lotto, R. B. (1996). Influences of the thalamus on the survival of subplate and cortical plate cells in cultured embryonic mouse brain. *J. Neurosci.* 16, 3247–3255.

Ragozzino, M. E. (2007). The contribution of the medial prefrontal cortex, orbitofrontal cortex, and dorsomedial striatum to behavioral flexibility. *Ann. N.Y. Acad. Sci.* 1121, 355–375. doi: 10.1196/annals.1401.013

Ragozzino, M. E., Detrick, S., and Kesner, R. P. (1999). Involvement of the prelimbic-infralimbic areas of the rodent prefrontal cortex in behavioral flexibility for place and response learning. *J. Neurosci.* 19, 4585–4594.

Ramos-Chavez, L. A., Rendon-Lopez, C. R., Zepeda, A., Silva-Adaya, D., Del Razo, L. M., and Gonsebatt, M. E. (2015). Neurological effects of inorganic arsenic exposure: altered cysteine/glutamate transport, NMDA expression and spatial memory impairment. *Front. Cell. Neurosci.* 9:21. doi: 10.3389/fncel.2015.00021

Rasse, T. M., Fouquet, W., Schmid, A., Kittel, R. J., Mertel, S., Sigrist, C. B., et al. (2005). Glutamate receptor dynamics organizing synapse formation *in vivo*. *Nat. Neurosci.* 8, 898–905. doi: 10.1038/nn1484

Rios, R., Zarazua, S., Santoyo, M. E., Sepulveda-Saavedra, J., Romero-Diaz, V., Jimenez, V., et al. (2009). Decreased nitric oxide markers and morphological changes in the brain of arsenic-exposed rats. *Toxicology* 261, 68–75. doi: 10.1016/j.tox.2009.04.055

Rocha-Amador, D., Navarro, M. E., Carrizales, L., Morales, R., and Calderon, J. (2007). Decreased intelligence in children and exposure to fluoride and arsenic in drinking water. *Cad. Saude Publica* 23 (Suppl. 4), S579–S587. doi: 10.1590/s0102-311x2007001600018

Rodriguez, V. M., Carrizales, L., Jimenez-Capdeville, M. E., Dufour, L., and Giordano, M. (2001). The effects of sodium arsenite exposure on behavioral parameters in the rat. *Brain Res. Bull.* 55, 301–308. doi: 10.1016/S0361-9230(01)00477-4

Rodriguez, V. M., Carrizales, L., Mendoza, M. S., Fajardo, O. R., and Giordano, M. (2002). Effects of sodium arsenite exposure on development and behavior in the rat. *Neurotoxicol. Teratol.* 24, 743–750. doi: 10.1016/S0892-0362(02)00313-6

Rosado, J. L., Ronquillo, D., Kordas, K., Rojas, O., Alatorre, J., Lopez, P., et al. (2007). Arsenic exposure and cognitive performance in Mexican schoolchildren. *Environ. Health Perspect.* 115, 1371–1375. doi: 10.1289/ehp.9961

Ross, M. G., Desai, M., Guerra, C., and Wang, S. (2005). Prenatal programming of hypernatremia and hypertension in neonatal lambs. *Am. J. Physiol. Regul. Integr. Comp. Physiol.* 288, R97–R103. doi: 10.1152/ajpregu.00315.2004

Schreiber, T., Gassmann, K., Gotz, C., Hubenthal, U., Moors, M., Krause, G., et al. (2010). Polybrominated diphenyl ethers induce developmental neurotoxicity in a human *in vitro* model: evidence for endocrine disruption. *Environ. Health Perspect.* 118, 572–578. doi: 10.1289/ehp.0901435

Tomasini, M. C., Beggiato, S., Ferraro, L., Tanganelli, S., Marani, L., Lorenzini, L., et al. (2012). Prenatal exposure to 2,3,7,8-tetrachlorodibenzo-p-dioxin produces alterations in cortical neuron development and a long-term dysfunction of glutamate transmission in rat cerebral cortex. *Neurochem. Int.* 61, 759–766. doi: 10.1016/j.neuint.2012.07.004

Tsukahara, S., Tsuda, M. C., Kurihara, R., Kato, Y., Kuroda, Y., Nakata, M., et al. (2011). Effects of aromatase or estrogen receptor gene deletion on masculinization of the principal nucleus of the bed nucleus of the stria terminalis of mice. *Neuroendocrinology* 94, 137–147. doi: 10.1159/000327541

Valencia, E., Gil, A., Zapico, R. M., Garcia Rodriguez, M. C., Pintado, V., Lopez Dupla, M., et al. (1992). [Azidothymidine in the treatment of patients with human immunodeficiency virus infection and persistent generalized adenopathies]. *An. Med. Interna* 9, 531–537.

Valentin, V. V., Dickinson, A., and O'doherty, J. P. (2007). Determining the neural substrates of goal-directed learning in the human brain. *J. Neurosci.* 27, 4019–4026. doi: 10.1523/JNEUROSCI.0564-07.2007

Van De Werd, H. J., Rajkowska, G., Evers, P., and Uylings, H. B. (2010). Cytoarchitectonic and chemoarchitectonic characterization of the prefrontal cortical areas in the mouse. *Brain Struct. Funct.* 214, 339–353. doi: 10.1007/s00429-010-0247-z

Waalkes, M. P., Ward, J. M., Liu, J., and Diwan, B. A. (2003). Transplacental carcinogenicity of inorganic arsenic in the drinking water: induction of hepatic, ovarian, pulmonary, and adrenal tumors in mice. *Toxicol. Appl. Pharmacol.* 186, 7–17. doi: 10.1016/S0041-008X(02)00022-4

Wang, Y., Zhao, F., Liao, Y., Jin, Y., and Sun, G. (2012). Arsenic exposure and glutamate-induced gliotransmitter release from astrocytes. *Neural Regen. Res.* 7, 2439–2445. doi: 10.3969/j.issn.1673-5374.2012.31.005

Wasserman, G. A., Liu, X., Parvez, F., Ahsan, H., Factor-Litvak, P., Kline, J., et al. (2007). Water arsenic exposure and intellectual function in 6-year-old children in Araihazar, Bangladesh. *Environ. Health Perspect.* 115, 285–289. doi: 10.1289/ehp.9501

WHO (2008). *"Guidelines for drinking-water quality, recommendations,"* in *Incorporating 1st and 2nd Addenda. Vol. 1, 3rd Edn* (Geneva: World Health Organization), 306–308b. Available online at: http://www.who.int/water_sanitation_health/dwq/gdwq3/en/index.html

Willhite, C. C., and Ferm, V. H. (1984). Prenatal and developmental toxicology of arsenicals. *Adv. Exp. Med. Biol.* 177, 205–228. doi: 10.1007/978-1-4684-4790-3_9

Wong, H. K., Fricker, M., Wyttenbach, A., Villunger, A., Michalak, E. M., Strasser, A., et al. (2005). Mutually exclusive subsets of BH3-only proteins are activated by the p53 and c-Jun N-terminal kinase/c-Jun signaling pathways during cortical neuron apoptosis induced by arsenite. *Mol. Cell. Biol.* 25, 8732–8747. doi: 10.1128/MCB.25.19.8732-8747.2005

Yan, C., Yang, T., Yu, Q. J., Jin, Z., Cheung, E. F., Liu, X., et al. (2015). Rostral medial prefrontal dysfunctions and consummatory pleasure in schizophrenia: a meta-analysis of functional imaging studies. *Psychiatry Res.* 231, 187–196. doi: 10.1016/j.pscychresns.2015.01.001

Yang, D., Liang, C., Jin, Y., and Wang, D. (2003). [Effect of arsenic toxicity on morphology and viability of enzyme in primary culture of rat hippocampal neurons]. *Wei Sheng Yan Jiu* 32, 309–312.

Zhang, H., Fan, Y., Xia, F., Geng, C., Mao, C., Jiang, S., et al. (2011). Prenatal water deprivation alters brain angiotensin system and dipsogenic changes in the offspring. *Brain Res.* 1382, 128–136. doi: 10.1016/j.brainres.2011.01.031

Conflict of Interest Statement: The authors declare that the research was conducted in the absence of any commercial or financial relationships that could be construed as a potential conflict of interest.

Nucleic Acids Research Advance Access published March 4, 2016

doi: 10.1093/nar/gkw113

Bidirectional promoters link cAMP signaling with irreversible differentiation through promoter-associated non-coding RNA (pancRNA) expression in PC12 cells

Naoki Yamamoto[1,2], Kiyokazu Agata[2], Kinichi Nakashima[1] and Takuya Imamura[1,*]

[1]Department of Stem Cell Biology and Medicine, Graduate School of Medical Sciences, Kyushu University, Japan and [2]Department of Biophysics, Graduate School of Science, Kyoto University, Japan

Received November 18, 2015; Revised January 25, 2016; Accepted February 16, 2016

ABSTRACT

Bidirectional promoters are the major source of gene activation-associated noncoding RNA (ncRNA). PC12 cells offer an interesting model for understanding the mechanism underlying bidirectional promoter-mediated cell cycle control. Nerve growth factor (NGF)-stimulated PC12 cells elongate neurites, and are in a reversible cell-cycle-arrested state. In contrast, these cells irreversibly differentiate and cannot re-enter the normal cell cycle after NGF plus cAMP treatment. In this study, using directional RNA-seq, we found that bidirectional promoters for protein-coding genes with promoter-associated ncRNA (pancRNA) were enriched for cAMP response element consensus sequences, and were preferred targets for transcriptional regulation by the transcription factors in the cAMP-dependent pathway. A spindle-formation-associated gene, *Nusap1* and *pancNusap1* were among the most strictly co-transcribed pancRNA–mRNA pairs. This pancRNA–mRNA pair was specifically repressed in irreversibly differentiated PC12 cells. Knockdown (KD) and overexpression experiments showed that *pancNusap1* positively regulated the *Nusap1* expression in a sequence-specific manner, which was accompanied by histone acetylation at the *Nusap1* promoter. Furthermore, *pancNusap1* KD recapitulated the effects of cAMP on cell cycle arrest. Thus, we conclude that pancRNA-mediated histone acetylation contributes to the establishment of the cAMP-induced transcription state of the *Nusap1* locus and contributes to the irreversible cell cycle exit for terminal differentiation of PC12 cells.

INTRODUCTION

Many long noncoding RNAs (lncRNAs) have been shown to be transcribed from the mammalian genome, and have emerged as key players of many cellular functions (1–4). The majority of non-coding RNAs (ncRNAs) involved in mRNA metabolism in mammals have been thought to downregulate the corresponding mRNA expression level in a pre- or post-transcriptional manner by forming ncRNA–mRNA duplex structures (2,5). However, several studies have shown that some lncRNAs function without forming RNA–RNA duplexes (6–9).

The transcripts derived from bidirectional promoters include not only protein-coding mRNAs, but also lncRNAs, and a significant proportion of such lncRNAs derived from bidirectional promoters are expressed in tissue-specific manners (10,11). We previously showed that functional polyA+, long (>200 bp) ncRNAs derived from bidirectional promoters, named promoter-associated ncRNAs (pancRNAs), are expressed in tissue-specific manners and function in the activation of their partner genes (7,8,11,12). For example, in mice, microinjection of siRNA against the abundant pancRNA partner of interleukin 17d (*Il17d*) mRNA at the 1-cell stage caused embryonic lethality, which was rescued by supplying IL17D protein *in vitro* at the 4-cell stage (7). Thousands of pancRNAs are generated by transcription of the antisense strand and exhibit expression changes coordinated with the expression of their cognate genes (11), making bidirectional promoters a major source of gene activation-associated ncRNA.

Transcriptional regulation by binding of transcription factors to the cAMP response element (CRE) downstream of cAMP signaling plays important roles in the cell differentiation process (13,14). Transcription factors that bind to CRE, such as CRE-binding protein (Creb) and CRE modulator (Crem), are activated by cAMP-dependent protein kinase (Pka)-mediated phosphorylation, and activate

*To whom correspondence should be addressed. Tel: +81 92 642 6196; Fax: +81 92 642 6561; Email: imamura@scb.med.kyushu-u.ac.jp
Present address: Naoki Yamamoto, Life Science Tokyo Advanced Research center (L-StaR), Hoshi University School of Pharmacy and Pharmaceutical Science, Japan.

gene expression by means of recruitment of coactivator paralogs CREB-binding protein (Cbp) and p300 (15,16). Transcription factors that bind to CRE can act not only as transcriptional activators but also as transcriptional repressors. Inducible cAMP early repressor (Icer) is generated from an alternative intronic promoter of *Crem*, and acts as a transcriptional repressor (17). Icer lacks the activation and kinase-inducible domains, but retains the DNA-binding domain (18,19), and therefore is a potent repressor of cAMP-induced transcription. In a different context, CREB1 forms a complex with p53, and then inhibits p53-mediated transcriptional activation of the MDM2 gene in a human cell line during glucose deprivation (20). It is noteworthy that, using chromatin immunoprecipitation (ChIP) coupled with massively parallel sequencing (ChIP-seq), Impey *et al.* demonstrated that phosphorylated Creb1 (pCreb1)-bound regions are enriched in the bidirectional promoters of annotated transcript pairs that are organized in a head-to-head arrangement on opposite strands (15). Thus, comprehensive analysis of bidirectional promoters may identify a set of transcripts that are upregulated and downregulated by cAMP and that play a role in defining the cell state. We hypothesize that certain pancRNAs derived from bidirectional promoters are upregulated or downregulated by a cAMP-dependent mechanism.

In this context, rat adrenal phaeochromocytoma-derived PC12 cells offer an interesting model for studying cAMP-dependent pancRNA functions in cell cycle regulation associated with differentiation. Nerve growth factor (NGF)-stimulated PC12 cells elongate neurites and are reversibly arrested, that is, they can resume efficient cell cycling when they are put back under proliferative conditions (21). In contrast, when PC12 cells are stimulated simultaneously with NGF and a cAMP analog, dibutyryl cAMP (db-cAMP), they cannot re-enter the cell cycle even after the removal of NGF and dbcAMP (22). This shows that irreversible differentiation of PC12 cells can be induced by a cAMP-dependent mechanism. A previous *in vivo* study showed that pharmacological activation of the cAMP pathway rescued impairment of neuronal differentiation of neural progenitors caused by brain-specific knockout of the *Nf1* gene in mice, suggesting that a cAMP-dependent mechanism is also required for the *in vivo* neuronal differentiation of neural progenitor cells (13). The cell cycle of terminally differentiated cells is repressed by a cAMP-dependent mechanism, but the underlying molecular mechanisms are unknown.

In this study, by comparing the transcriptome of NGF-differentiated (Ndiff) PC12 cells with that of NGF/cAMP-differentiated (NcAdiff) PC12 cells, we highlighted the critical importance of cell cycle regulation for the terminal differentiation of cells that cannot resume mitosis. We showed that a significant number of M-phase-associated genes were repressed in NcAdiff cells, compared to Ndiff cells. As expected, we found that a significant number of CREs were enriched in the thousands of newly identified bidirectional promoters for the expression of pancRNA–mRNA pairs. Here, we report that these bidirectional promoters were preferred targets for transcriptional regulation by the transcription factors in the cAMP-dependent pathway. Furthermore, among the pancRNA–mRNA pairs, a pancRNA (*pancNusap1*) at the *Nusap1* locus, which encodes a spindle-formation-associated gene, and *Nusap1* mRNA together play a functional role in the irreversible differentiation of PC12 cells. Artificial downregulation of the *pancNusap1* expression level recapitulated the cAMP-triggered morphological features and epigenetic state of the irreversibly differentiated PC12 cells.

MATERIALS AND METHODS

PC12 culture and differentiation

PC12 cells were maintained in high-glucose Dulbecco's modified Eagle's medium (DMEM) (WAKO) containing 10% horse serum (HS; SAFC Biosciences), 5% fetal bovine serum (FBS; Biowest), 100 units/ml penicillin (PhytoTechnology Laboratories), and 100 μg/ml streptomycin (MP Biomedicals) at 37°C in 5% CO_2. To induce differentiation, PC12 cells were placed on a collagen (Cellmatrix Type IV, Nitta Gelatin)-precoated dish at a density of 8000 cells/cm^2, and were cultured in high-glucose DMEM containing 1% HS, 0.5% FBS, 100 units/ml penicillin, 100 μg/ml streptomycin, 100 ng/ml NGF 2.5S (Millipore) or 50 ng/ml NGF 2.5S and 200 μM dibutyryl cAMP (SIGMA) for 7 days. During differentiation, cell culture medium was changed at day 3 and day 5. To observe the cell cycle resumption of differentiated PC12 cells, the differentiation medium was changed at day 7 to high-glucose DMEM containing 10% HS, 5% FBS and antibiotics. For doxycycline (Dox)-inducible pancRNA overexpression/knockdown (OE/KD) experiments, cells were incubated in the above medium containing 2 ng/ml Dox (Nacalai Tesque).

Immunocytochemistry

Immunocytochemistry was performed as follows: fixation with 4% paraformaldehyde (PFA) for 20 min in RT; washing with phosphate buffered saline (PBS) twice; permeabilization and blocking in PBS containing 0.1% Triton X-100 and 3% FBS in PBS for 30 min at RT; incubation with primary antibody diluted 1:500 in blocking solution for 2 h in RT; washing with PBS three times; incubation with Hoechst 33258 (Nacalai Tesque) and secondary antibody diluted 1:500 in PBS for 1 h in the dark at RT; washing with PBS three times. Imaging was performed using a Leica AF6000 microscope. As primary antibodies, chicken anti-GFP (AVES Labs), mouse anti-Ki67 (BD Biosciences) and rabbit anti-active Caspase 3 (R&D Systems) were used. As secondary antibodies, the following were used: CF647-conjugated anti-mouse IgG (Biotium) and CF647-conjugated anti-rabbit IgG (Biotium), FITC-conjugated anti-chick IgY (Biotium). For the EdU assay, cells were cultured with 10 μM EdU in Click-iT EdU Imaging Kits (Life Technologies) for 4 h, fixed with 4% PFA, permeabilized with 0.1% Triton-X and 3% FBS in PBS, and stained with Click-iT reaction buffer for 30 min at RT in the dark. After washing with PBS, primary and secondary staining were performed in the dark.

RNA analysis

To examine RNA expression, total RNA isolated with TRIzol reagent (Life Technologies) was treated with DNase

I (Life Technologies) and reverse-transcribed with oligo dT primer using the SuperScriptIII First-Strand Synthesis System (Life Technologies). Synthesized cDNAs were subjected to qPCR using a KAPA SYBR Fast qPCR Kit (KAPA Biosystems). The primers used in these analyses are listed in Supplementary Table S1.

Directional RNA-seq library preparation

Directional RNA-seq libraries were prepared as follows. RNA with RNA integrity number above 9.6, calculated using total RNA Pico Bioanalyzer chip (Agilent), was used for Directional RNA-seq library preparation. polyA+ RNA was purified twice from 15 μg of total RNA of each PC12 sample by using Sera-mag Magnetic Oligo (dT) Beads (Thermo Scientific). In each polyA+ RNA sample, the fraction of rRNA was confirmed to be <2% by using a Total RNA Pico Bioanalyzer chip. The polyA+ RNA was fragmented by heating at 94°C for 2 min in 1 × fragmentation buffer (Affymetrix), and then the RNA was purified with two volumes of Agencourt RNAclean XP (Beckman Coulter). Fragmented RNA was decapped with 5 U TAP (Epicenter), and then subjected to phenol:chloroform:isoamylalcohol (PCI) extraction and ethanol precipitation. Fragmented and decapped RNA was 3′-dephosphorylated using Antarctic phosphatase (NEB). The RNA was 5′-phosphorylated using T4 polynucleotide kinase (NEB). The modified RNA was cleaned up with an RNeasy MinElute kit (Qiagen), was ligated to NEBNext Multiplex 3′ SR Adaptor with T4 RNA ligase 2 truncated K277Q (NEB) at 4°C overnight, and was further ligated to NEBNext Multiplex 5′ SR Adaptor with T4 RNA ligase (Illumina) at 20°C for 1 h. cDNA was synthesized with specific RT primer and the SuperScriptIII First-Strand Synthesis System. After RNase H treatment, unincorporated primers in each cDNA library sample were removed by using AMPure XP (Beckman Coulter). Each cDNA was independently amplified with KAPA Hifi HS polymerase (Kapa Biosystems) and NEBNext Index 1, 8, 10 and 11 primers in NEBNext Multiplex Oligos for Illumina (NEB) to produce four replicates for each sample. Thermal-cycling conditions were as follows: 30 s at 98°C, 12 cycles of 98°C for 15 s, 62°C for 30 s and 72°C for 30 s, followed by 5 min at 72°C. The polymerase chain reaction (PCR) product was purified twice with AMPure XP. Illumina HiSeq 2000 was used to perform 50-bp single-end sequencing according to the manufacturer's instructions.

Data mining

To remove low quality reads and adaptor sequences (AGATCGGAAGAGCACACGTCTGAACTCCAGTCAC), the FASTX tool kit (http://hannonlab.cshl.edu/fastx_toolkit/index.html) was used as follows: Remove low quality reads (phred score <20); remove 3′-end multiplex adapter tag sequence; remove the reads shorter than 20 nt; remove low quality reads again. The raw reads from all PC12 samples resulted in a total of 517 million strand-specific reads. We mapped sequencing reads from each sample onto the rat Rn5 genome sequences except for random chromosome sequences using TopHat (v.2.0.8b, option: -g 1 –bowtie1) (23). RSeQC (24) was used for quality evaluation of the strandedness in our cDNA libraries. The read-enriched regions in each cell state were detected using MACS2 (v.2.0.10b, option: –nomodel –broad -g 2.57e9 -p 0.95) (25). All reads in biological replicates were merged and used as the input data for MACS2. Overlapping read-enriched regions between different cell states were merged to create one broad region using the mergeBed function of BEDTools (26). This resulted in 149 559 read-enriched regions (minimum length set to 300 nt). When a reference transcription start site (TSS) in the Rn5 genome assembly was overlapped with a read-enriched region, we defined the 5′-end of this region as the adjusted TSS in PC12 cell samples except for cases in which the 5′-end overlapped with another gene. The coding potentials of non-annotated transcripts and candidate-pancRNAs were estimated using the coding potential calculator (CPC) algorithm (27). For mRNA and ncRNA quantification, we counted the number of reads mapped to the exonic region of Ensembl protein-coding genes and read-enriched regions classified as non-annotated transcripts, respectively, followed by normalization using the iDEGES/edgeR methods and differential expression analyses using R package TCC (28).

For the correlation analysis in Figure 3C, Pearson correlation coefficients between the expression levels of novel transcripts and annotated protein-coding genes were calculated. In this analysis, randomly selected lncRNA and mRNA pairs were generated using the publicly available program (https://cell-innovation.nig.ac.jp/wiki/tiki-download_wiki_attachment.php?attId=5&download=y). For enrichment analysis of biological process ontology, differentially expressed genes were annotated using DAVID (29).

Enrichment analysis of CRE and Creb1 binding score in bidirectional promoter

For enrichment analysis of CREs, the locations of CREs were searched using the R package ChIPpeakAnno (option: min.score = '90%') (30) using Creb1 binding sequence data that is registered in the JASPAR database (ID = MA0018.2) (31).

For enrichment analysis of Creb1 binding score, the mouse Mm9 genome-mapped Creb1 ChIP-seq dataset of E16.5 mouse cortical neurons that had been maintained *in vitro* for 7 days obtained from Gene Expression Omnibus (acc. no GSM530185) (32) was converted to the corresponding dataset in the rat Rn5 genome using the UCSC LiftOver tool (http://hgdownload.cse.ucsc.edu/admin/exe). Similarly, the rat rn3 genome-mapped pCreb1 ChIP-seq dataset of PC12 cells 15 min after cAMP signal activation by forskolin (15), deposited as a supplementary data of a serial report (33), was converted to the corresponding dataset in the rat Rn5 genome using the UCSC LiftOver tool.

Chromatin immunoprecipitation (ChIP) analysis

For ChIP analysis, we generated Dox-inducible short hairpin RNA (shRNA)-expressing or pancRNA-expressing PC12 cell lines, as described later. Cells (about 4×10^5) in

a 10-cm Petri dish were fixed with 1% formaldehyde for 5 min at RT. Samples were placed on ice and washed twice with ice-cold PBS. Cells were harvested by scraping with 1 ml of resuspension solution (10% NaN_3, 2% FBS in 1 × PBS) and counted, and were centrifuged at 2000 g for 5 min at 4°C. Cell pellets were washed with 1 ml of ice-cold PBS, resuspended in lysis buffer containing 1% sodium dodecyl sulphate (SDS), 50 mM Tris–HCl [pH 8.0], 10 mM ethylenediaminetetraacetic acid (EDTA) [pH 8.0] and 1% protease inhibitor cocktail (Nacalai Tesque) at a concentration of 1 × 10^5 cells per 100 μl, kept on ice for 10 min, then sonicated to an average size of 500 bp using a Bioruptor (Diagenode). After centrifugation for 15 min at 15 000 rpm at 4°C, supernatants containing sonicated chromatin were transferred to fresh tubes and diluted 1:10 with ChIP dilution buffer (1.1% Triton X-100, 50 mM Tris–HCl [pH 8.0], 167 mM NaCl, 0.11% sodium deoxycholate, 1% protease inhibitor cocktail). Immunoreaction was performed overnight at 4°C with rotation. For each sample preparation, 5 × 10^4 cells and 1 μl of each antibody (anti-mouse-H3K4me3, anti-mouse-H3K9me3, anti-mouse-H3K27me3, anti-mouse-H3K27ac or anti-mouse-H3K9ac; Cosmo Bio) or mouse-IgG (Santa Cruz) as a negative control were used. For ChIP for pCreb1 and Icer, 3 × 10^6 cells and 4 μg of each antibody (anti-rabbit-pCreb1(Ser133); Cell Signaling Technology, anti-rabbit-Crem(X-12); Santa Cruz) or rabbit-IgG (Santa Cruz) as a negative control were used. Immune complexes were captured with 10 μl of M-280 sheep anti-mouse IgG (Life Technologies) or 40 μl of M-280 sheep anti-rabbit IgG (Life Technologies) for 4 h at 4°C. After the beads were washed once with ice-cold RIPA buffer (0.1% SDS, 1% Triton X-100, 50 mM Tris–HCl [pH 8.0], 1 mM EDTA [pH 8.0], 150 mM NaCl, 0.1% sodium deoxycholate), once with ice-cold high-NaCl RIPA buffer (0.1% SDS, 1% Triton X-100, 50 mM Tris–HCl [pH 8.0], 1 mM EDTA [pH 8.0], 300 mM NaCl, 0.1% sodium deoxycholate) and twice with ice-cold TE (10 mM Tris–HCl [pH 8.0], 1 mM EDTA [pH 8.0]), formaldehyde cross-linking was reversed by overnight incubation with 200 μl of ChIP elution buffer (0.5% SDS, 10 mM Tris–HCl [pH 8.0], 5 mM EDTA [pH 8.0], 300 mM NaCl) at 65°C overnight. The immunoprecipitated samples and the same amount of chromatin fragments without IP (input) were treated with proteinase K for 1 h at 55°C, further treated with RNase A (Thermo Scientific) for 30 min at 37°C, and purified by PCI extraction and ethanol precipitation. DNA was resuspended in 20 μl of sterile water and used as a template for quantitative PCR with specific primers (see Supplementary Table S1). The results from three independent experiments were averaged.

Bisulfite sequencing

To determine the DNA methylation profiles of the *Nusap1* promoter regions, genomic DNAs were subjected to the bisulfite reaction using a MethylCode Kit (Life Technologies) according to the manufacturer's instructions. Each bisulfite-treated genome was amplified using AmpliTaq Gold 360 Master Mix (Life Technologies) or LA Taq (TaKaRa) with the primers listed in Supplementary Table S3. Each PCR product was cloned into pGEM T-easy (Promega) and 8 randomly picked clones were sequenced.

Plasmid construction and lentivirus production

Lentiviral vectors pLLX and pLEMPRA (34) were generously provided by Drs Z. Zhou and M. E. Greenberg.

For knockdown experiments, pLLX was used to enable the simultaneous expression of the shRNA and EGFP RNA under the control of U6 and ubiquitin-C promoters, respectively. The sh-RNA oligos were inserted into the HpaI and XhoI sites of pLLX (see Supplementary Table S2).

For rescue experiments, pLEMPRA was used to enable the simultaneous expression of the shRNA and EGFP-IRES-*Nusap1* under the control of U6 and ubiquitin-C promoters, respectively. A FLAG-tagged rat *Nusap1* expression lentiviral vector was constructed by inserting *Nusap1* cDNA between the EcoRI and AscI sites, and inserting the *sh-pancNusap1* sequence between the HpaI and XhoI sites of pLEMPRA (see Supplementary Table S2).

For conditional *pancNusap1*-OE or -KD experiments, we employed the lentivirus-based pSLIK_Neo vector system (Addgene), which allows tight Dox-inducible, RNA polymerase II (RNAPII)-mediated transcription of a gene of interest, and co-expression of a Neomycin selection gene (35). The panc*Nusap1* fragments (−1685 to −323 relative to the TSS of *Nusap1*), isolated by genomic PCR with specific primers (see Supplementary Table S2), were inserted into the SacII and XbaI sites of the entry vector pEN_TmiRc3 (Addgene). The annealed *sh-pancNusap1* oligo (see Supplementary Table S2) was inserted between the HpaI and XhoI sites of pEN_TmiRc3. Recombination of pEN_TmiRc3 and pSLIK_Neo was performed using the LR Clonase Enzyme Mix (Life Technologies) to obtain *pancNusap1*- or *sh-pancNusap1*-expressing vectors according to manufacturer's instructions. We confirmed that Dox-inducible expression of *sh-pancNusap1* successfully caused a reduction of *pancNusap1* expression in the PC12 cell line (Supplementary Figure S1).

HEK 293T cells were used as producers of lentiviruses, and were cultured in high-glucose DMEM (Nacalai Tesque) containing 10% FBS (Biowest) and antibiotics. The expression vector was transfected along with third-generation lentiviral packaging and pseudotyping plasmids (36) using PEI-MAX (COSMO BIO). Ten micrograms of pSLIK, pLLX or pLEMPRA plasmid, 3 μg of the packaging plasmid pCAG-HIVgp and 3 μg of pCMV-VSV-G-RSV-Rev were diluted in 500 μl of Opti-MEM (Gibco) and used for cells in a 10-cm-diameter dish. The medium was replaced after 12 h of transfection. The virus-containing supernatant was collected 48 h later, and the virus was concentrated by centrifugation at 6000 *g* overnight at 4°C, and used for the manipulation of *pancNusap1* or *Nusap1* expression in PC12 cells.

RESULTS

Cell cycle arrest was observed in the irreversible differentiation of NGF/cAMP-differentiated PC12 cells

Clear morphological differences were observed here between Ndiff and NcAdiff cells, as previously documented in the literature (22). NcAdiff cells could be distinguished from Ndiff cells by the thickening of neurites and increase in cell soma size of the former (Figure 1A). To ascertain